Earth and Environmental Sciences

Interface Phenomena

Catalysis of PAH biodegradation by humic acid shown in synchtrotron infrared studies
Holman, H.-Y., K. Nieman, D.L. Sorensen, C.D. Miller, M.C. Martin, T. Borch, W.R. McKinney, R.C. Sims

Investigation of interfacial chemistry of microorganisms
Ingram, J.C., D.E. Cummings, H.-Y. Holman, M.Downing

Microscale characterization of the location and association of TNT in soils
Ghosh, U., R.G. Luthy

New IR microscope and bench installed at BL 1.4
Martin, M.C., H.-Y. Holman, W.R. McKinney

Spatial distribution of bacteria on basalt using SR-FTIR
Kauffman, M.E., H.-Y. Holman, R.M. Lehman, M.C. Martin

Surface spectroscopy of nano-scale reactions in aqueous solution
Pecher, K.H., B. Tonner

Catalysis of PAH Biodegradation by Humic Acid Shown in Synchrotron Infrared Studies

Hoi-Ying N. Holman,[1] Karl Nieman,[2] Darwin L. Sorensen,[2] Charles D. Miller,[3] Michael C. Martin,[4] Thomas Borch,[5] Wayne R. McKinney,[4] and Ronald C. Sims[2]
[1]Center for Environmental Biotechnology, Lawrence Berkeley National Laboratory, Berkeley, CA 94720
[2]Utah Water Research Laboratory, Utah State University, Logan, UT 84321
[3]Biology Department, Utah State University, Logan, UT 84321
[4]Advanced Light Source Division, Lawrence Berkeley National Laboratory, Berkeley, CA 94720
[5]Center for Biofilm Engineering, Montana State University, Bozeman, MT 59717

INTRODUCTION

Humic acids (HAs) are complex organic molecules produced by the decomposition of plant and animal remains in soils. The surfactant-like micellar microstructure of HA is thought to accelerate the degradation of polycyclic aromatic hydrocarbons (PAHs) by enhancing PAH solubility, thereby increasing the PAH bioavailability to microorganisms. Despite abundant evidence that HA is important in the bioremediation of several anthropogenic pollutants, its role in the detoxification of PAHs by microbes remains uncertain.

Previous inconclusive results motivate a novel approach to the study of this important biogeochemical process. We used SR-FTIR spectromicroscopy to examine the effects of soil HA on biodegradation of the model PAH pyrene in the presence of a colony of Mycobacterium sp. JLS, on a mineral surface in an unsaturated environment. Infrared spectra measured during the onset and progress of biodegradation constitute the first microscopic study of this process to be made in real time.

PROCEDURE

SR-FTIR spectra were obtained at ALS BL1.4.3 from samples of M. sp. JLS as they degraded pyrene on magnetite surfaces, with and without the addition of Elliott Soil Humic Acid (ESHA). The pyrene-degrading microorganism M. sp. JLS is a gram-positive, rod-shape bacterium (GenBank accession no. AF387804); our samples were recently isolated from PAH-contaminated soil at the Libby Groundwater Superfund Site in Libby, Montana, USA. Our mineral substrates were freshly cleaved and sonicated surfaces of small chips (less than 1 cm in diameter) of magnetite rock from Minerals Unlimited of Ridgecrest, CA.

The time-dependent pyrene biodegradation experiments were began by adding 2.5 ml of cell suspension (~1.5 × 108 cells/milliliter) of M. sp. JLS onto the prepared magnetite chips. A custom IR microscope-stage mini-incubator was used to maintain the proper growth conditions for M. sp. JLS, while allowing *in situ* FTIR spectromicroscopy measurements. For abiotic controls, no M. sp. JLS was applied. Non-overlapping IR spectral markers were selected to monitor each component.

RESULTS

Figure 1 summarizes the time series of infrared spectra obtained by repeatedly measuring the same location on each pyrene-coated sample for more than a month. Since the sample surface is different for each experiment, the absolute value of absorbance can vary. However by

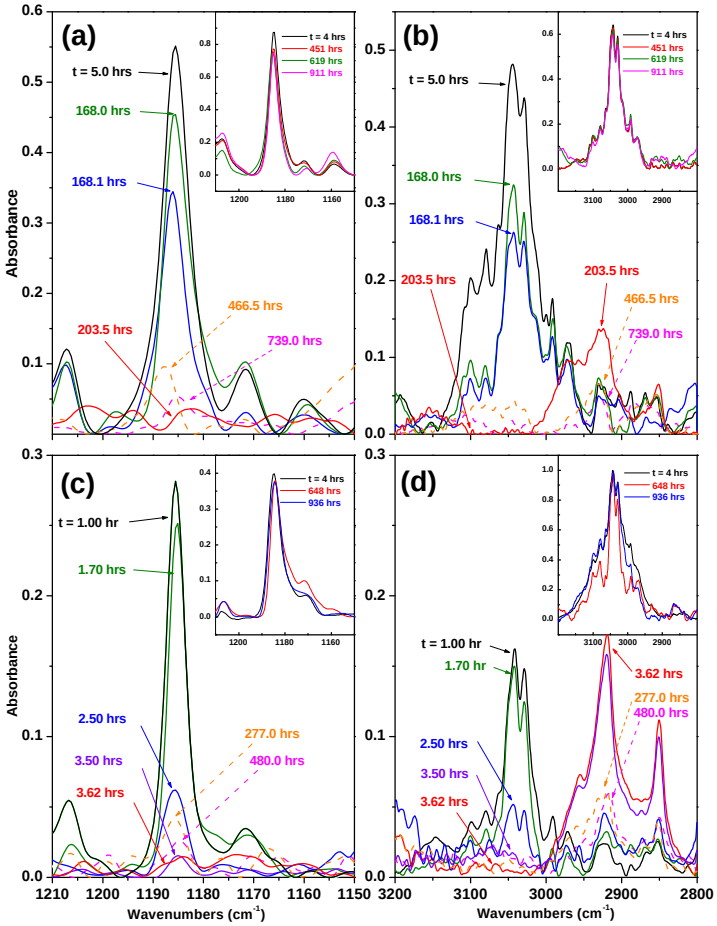

Figure 1. Time series of SR-FTIR absorption bands corresponding to pyrene and biomass formation following the degradation of pyrene by Mycobacterium sp. JLS on magnetite surfaces. Panels (a) and (b) are without ESHA; panels (c) and (d) are with ESHA. (a) and (c) show a pyrene absorption band at 1185 cm^{-1}. (b) and (d) show a pyrene doublet at 3044 and 3027 cm^{-1} and biomass IR absorption at 2921 and 2850 cm^{-1}. Inserts are abiotic control experiments.

monitoring the same position on each sample individually, the changes in absorption are quantitative. Over a similar period, the infrared spectra obtained from samples free of pyrene did not show statistically significant changes.

For samples without ESHA, pyrene biodegradation starts very slowly, and about 168 hours elapse before significant changes are observed. Biodegradation then proceeds quickly, and all the observed pyrene is completely degraded within the next 35 hours. As the pyrene peaks in the spectra disappear, we observe an increase in the biomass IR absorption peaks, implying concurrent biomass formation during the consumption of pyrene (Fig. 1, panels (a) and (b)). By contrast, the biodegradation of pyrene on samples with ESHA begins almost immediately (~1 hour) after the introduction of M. sp. JLS (Fig. 1, panels (c) and (d)). The degradation of the observed pyrene is complete by the fourth hour. Again we detect an increase in biomass absorption during the later stage of the pyrene degradation, which implies that biomass formation is concurrent with the consumption of pyrene.

Figure 2 displays pyrene concentration and biomass versus time under three different conditions, as measured by associated spectral absorbances normalized to remove surface effects as described above. Abiotic results show that pyrene remains on the mineral surface, with only slow removal mechanisms. Pyrene degradation by M. sp. JLS without ESHA did not proceed until ~ 170 hours after the introduction of the bacteria, followed by a rapid decrease of pyrene and a rapid increase of biomass within the next thirty-five hours, as described earlier. After the pyrene was depleted the biomass signal significantly decreased, presumably as the M. sp. JLS bacteria transformed themselves into ultramicrocells, a starvation-survival strategy commonly observed among bacteria in oligotrophic environments. In the presence of ESHA, pyrene biodegradation begins within an hour and the observed pyrene is depleted by the end of the fourth hour, with a concurrent increase of biomass. It is likely that the water-insoluble pyrene is solubilized into cores of ESHA pseudo-micelles and therefore becomes available for bacterial consumption.

Over longer times, IR absorption bands of pyrene on magnetite surfaces showed a slight increase and decrease. The increase is probably due to pyrene diffusing from pyrene trapped in

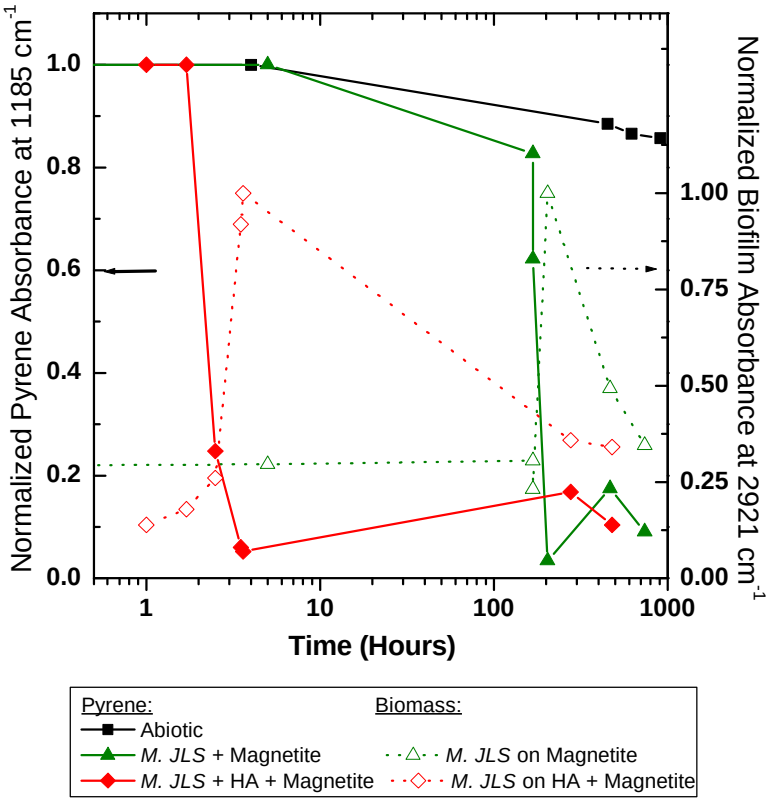

Figure 2. Summary of IR results showing that pyrene degradation occurs much faster when ESHA is present (note the log scale on the time axis). The color scheme is black for abiotic, green for biotic without ESHA, and red for biotic with ESHA. The solid lines correspond to pyrene and the dotted lines correspond to the biomass.

micropores of the magnetite and/or neighboring surfaces of higher pyrene concentration. Thus the first wave of rapid depletion of pyrene by M. sp. JLS set up a diffusion gradient from the pyrene-containing micropores toward the bacterial colony, leading to a subsequent small increase in pyrene concentration. For the surface containing ESHA, the biomass remained almost constant over a period of more than 200 hours, indicating that the flux of pyrene from the micropores was sufficient to maintain the bacterial colony. For the surface free of ESHA, there is little evidence of the presence of a quasi-steady state biomass.

DISCUSSION

Our results have significant implications for the bioremediation of contaminated soils. In many PAH-contaminated sites, bioremediation is specified by the U.S. Environmental Protection Agency as the preferred remedial technology. Bioremediation of PAH-contaminated soils is often limited, however, by the low solubility of PAH, which inhibits microbial uptake. Adding synthetic surfactants to enhance PAH solubility may be toxic to natural microorganisms and further inhibit bioremediation. Based on results reported here, a potential alternative in unsaturated soil environments may be the application of natural HA to accelerate the biodegradation of PAH.

SR-FTIR spectromicroscopy can assess real-time interactions between multiple constituents in contaminated soils. Combined with conventional mineralization measurements, which monitor respiration through carbon dioxide production, SR-FTIR spectromicroscopy is a powerful tool for evaluating bioremediation options and designing bioremediation strategies for contaminated vadose zone environments.

A longer version of this work will be published in Environmental Science and Technology, 2002.

This work was supported by the Director, Office of Energy Research, Office of Basic Energy Sciences, Materials Science Division, of the U.S. Department of Energy under Contract No. DE-AC03-76SF00098.

Principal investigator: Hoi-Ying N. Holman, Lawrence Berkeley National Laboratory. Email: hyholman@lbl.gov. Telephone: 510-486-5943.

Investigation of Interfacial Chemistry of Microorganisms

Jani C. Ingram,[1] David E. Cummings,[1] Hoi-Ying Holman,[2] and Matthew Downing[3]
[1]Idaho National Energy and Environmental Laboratory, ID
[2]Lawrence Berkeley National Laboratory, CA
[3]Shawnee High School, NJ

INTRODUCTION

Remediation of Department of Energy (DOE) sites contaminated with toxic metals and radionuclides is a complex and costly problem. Several bioremediation strategies currently being explored exploit the metabolism of naturally-occurring dissimilatory metal-reducing bacteria (DMRB). These bacteria catalyze the mobilization of some metal oxide-associated trace elements and the precipitation of many otherwise soluble metals and radionuclides. Our recent work centers on the effects of co-contaminating trace metals on the microbe-mineral interface.

RESULTS

Secondary ion mass spectrometry (SIMS) and synchrotron radiation Fourier transform infrared spectroscopy (SR-FTIR) were applied to examine biochemical changes incurred at the surface of Shewanella putrefaciens cells due to exposure to soluble arsenic. Cells responded to the insult with altered membrane fatty acids (observed by SIMS) and exopolysaccharide production (observed by SR-FTIR).

SR-FTIR at ALS beamline 1.4.3 was used to analyze *S. putrefaciens* cells with and without exposure to 100 mM As(V). The main difference between the spectra of stationary phase cells was the clear lack of a broad peak associated with carbohydrates in the As-exposed cells that was present in the unexposed cells (Figure below). In its place were two distinct peaks indicative of phosphodiester bonds. Phosphodiester bonds are abundant in cell membranes, forming the junction between glycerol and fatty acids. Cell surface carbohydrates likely indicate either a capsule (exopolysaccharides), or common membrane lipids called lipopolysaccharides (LPS). The role of the capsule is especially important in nature, where it can aid the cell in its defense against viruses, hydrophobic toxins such as detergents, and dessication. In addition, it has been implicated in the attachment of some microorganisms to solid substrates. An impaired ability to form exopolysaccharides would likely limit the cells competitive fitness in nature. The LPS may be largely responsible for the net negative charge on the cell surface, implicated in attachment, metal binding, and nutrient transport across the outer membrane. Additionally, the LPS may stabilize the membrane's physical shape and structure. An impaired LPS would also put the cells at a disadvantage in the environment.

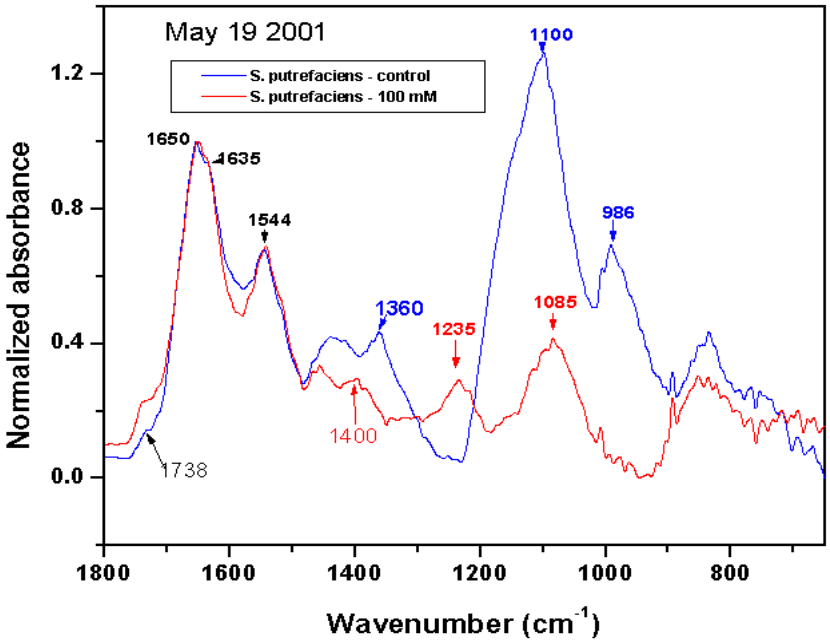

This work was supported by Idaho National Engineering and Environmental Laboratory.

Principal investigator: Jani C. Ingram, Idaho National Engineering & Environmental Laboratory (INEEL), Phone: (208) 526-0739, Fax: (208) 526-8541, email: uoa@inel.gov

Microscale Characterization of the Location and Association of TNT in Soils

U. Ghosh and R.G. Luthy
Department of Civil and Environmental Engineering, Stanford University, Stanford, CA 94305-4020

INTRODUCTION:

Numerous ammunition manufacturing facilities and ammunition testing sites across the world are faced with environmental problems associated with soils contaminated with trinitrotoluene (TNT) and other nitroaromatic compounds. Although a number of TNT treatment technologies have been developed recently [1,2], these techniques do not result in a high degree of mineralization of the explosive compounds present. Thus, a significant part of the contaminant mass remains in the soil as residues of the original contamination. The acceptance of cost-effective treatment techniques depends on better understanding of the stabilization of TNT and its nitroaromatic transformation products in soil. The chemical and biological availability of TNT residues in soil is determined primarily by the physical and chemical form in which TNT remain in soils. Reduction of TNT produces aminonitrotoluenes, which may covalently bond irreversibly with quinones, and reversibly with hydroquinones. Such transformation of molecular structure is implicated in making TNT transformation products unavailable for further degradation [3]. However, TNT residue may also be present in a solid form in soils, especially at former production facilities. Solid TNT particles may create a toxic zone in the vicinity thereby making biodegradation difficult. Thus it is important to understand the microscale nature of TNT residues found in contaminated soils.

In our previous work, microscale analytic techniques were used successfully to demonstrate the preferential binding of polycyclic aromatic hydrocarbons (PAHs) on coal-derived particles in sediment [4,5]. We showed in that work that PAH sorption on coal-derived particles is associated with minimal biodegradation, slow release rates, and high desorption activation energies, while PAH sorption on clay/silt particles is associated with significant potential biodegradability, relatively fast release rates, and lower desorption activation energies.

The primary focus of the current work is to develop microscale analytic techniques to assess whether crystalline TNT may exist in impacted soils and to apply these techniques to determine whether the presence of crystalline or pure TNT in soil may explain differences in biotreatability of TNT-impacted soils from the field.

RESULTS AND DISCUSSION:

The focus of this research is to develop methods to permit the identification at the particle and sub-particle scale whether solid-phase, crystalline TNT, or crystalline TNT transformation products exists in field soils. Infrared spectromicroscopy available at beamline 1.4 was used to detect the presence of solid TNT in contaminated soils. Although the fate of TNT and its transformation products in soil has been the subject of numerous investigations, important questions remain on whether pure solid TNT may account for an untreatable fraction of TNT in field samples. The hypothesis is that crystalline or pure TNT is toxic to microorganisms and not easily biotreatable and that differences in biotreatment of TNT-impacted soil may depend on whether the TNT is present as sorbed versus solid, crystalline form. Soil samples were obtained from two ammunition manufacturing facilities. Soils from these field sites are currently being

tested for possible application of biotreatment technologies. Half a gram of each soil was spread on red clay mounted on a microscope slide. IR analysis was carried out in the reflectance mode. In our investigations using IR spectromicroscopy we observed the presence of significant quantities of residual crystalline TNT embedded in both soil samples. We could identify solid TNT based on the unique spectral characteristics of the nitro groups present in TNT. As shown in Figure 1, strong IR absorbance peaks near 1550 and 1350 wavenumbers are indicative of the asymmetric and symmetric stretch vibrations of the NO_2 groups present in the TNT molecules. To illustrate the physical location and form of the solid TNT particles, a representative soil agglomerate containing solid TNT was investigated for TNT presence using line scanning as shown in Figure 2. Multiple spots along a straight line through the TNT spot were analyzed in the IR spectromicroscope. As shown in Figure 2, the two absorbance peaks for the nitro groups show up when the scan passes through the TNT spot in the image shown on top. The rest of the soil barely shows any appreciable TNT signal. Thus, the residual TNT seems to be present predominantly in the solid particulate form. A light-microscope image of the solid TNT spot reveals a crystalline structure as shown in Figure 2. A unique finding in our work using IR spectromicroscopy is the direct measurement of residual crystalline TNT embedded in soil as opposed to TNT sorbed on mineral or organic matter. This finding of the microscale nature of TNT residuals in field materials has a major implication on its availability and toxicity. Current work in this research is investigating the effect of crystalline TNT on biological and chemical treatment methods. We are investigating the behavior of TNT degrading organisms near the vicinity of TNT crystals in soil using live-dead staining procedures and visualization through laser confocal microscopy. Results from this research will provide important information on the particle and sub-particle locations of solid, crystalline TNT and whether this accounts for the variability in biotreatment of TNT.

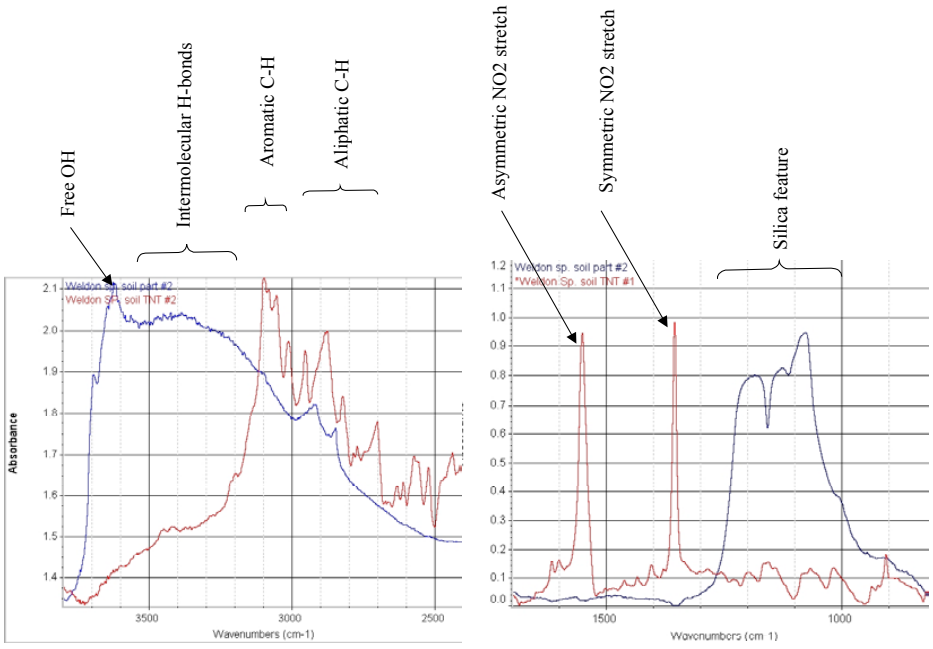

Figure 1. Results of experiments conducted at Beamline 1.4.2 illustrating the use of IR spectromicroscopy to identify the location of TNT micro-crystals present in contaminated soil from an ammunition manufacturing facility. The red line shows the absorbance spectra of the TNT crystals, and the blue line shows the absorbance spectra of soil.

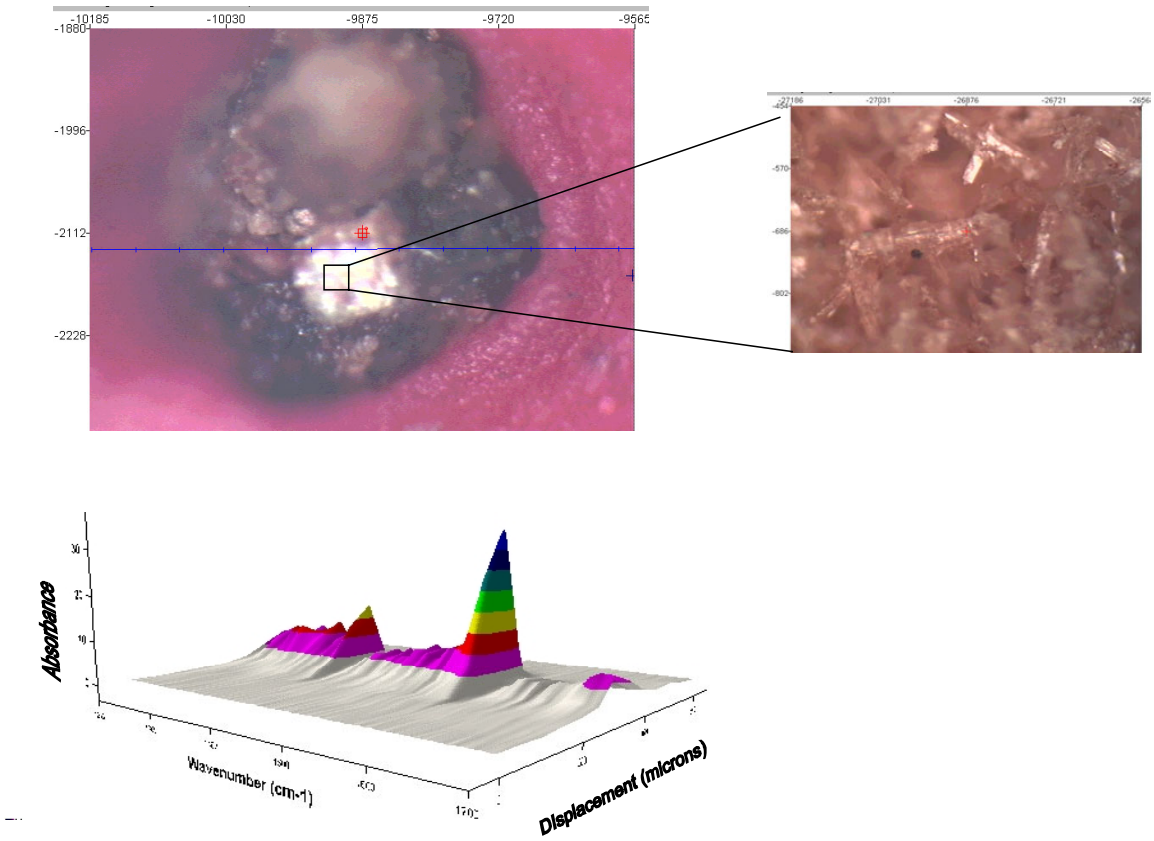

Figure 2. Top picture shows a soil particle with a white crystalline spot that was identified as crystalline TNT based on IR spectral map shown below. Contour map below shows IR absorbance along the blue line across the soil particle. The two prominent NO_2 stretch vibrations indicate a strong presence of TNT in the white spot. Image on the right shows a magnified image of the crystalline nature of TNT seen embed in the soil particle.

REFERENCES:

1. Daun, G.; H. Lenke; M. Reuss; H-J. Knackmuss. Environ. Sci. Technol. **33**, 2617, 1998.
2. Pennington, J.C.; C.A. Hayes; K.F. Myers; M. Ochman; D. Gunnison; D.R. Felt; E.F. McCormick. Chemosphere **30**, 429, 1995.
3. Sheremata, T.W.; S. Thiboutot; G. Ampleman; L. Paquet; A. Halasz; J. Hawari. Environ. Sci. Technol. **32**, 4002, 1998.
4. U. Ghosh, R.G. Luthy, J.S. Gillette and R.N. Zare. Environ. Sci. Technol, **34**, 1729, 2000.
5. J.W. Talley U. Ghosh, S.G. Tucker, J.S. Furey, and R. G. Luthy. Environ. Sci. Technol, (in press).

Funding for this work was provided by the US Army Waterways Experiment Station, Vicksburg, MS.

Contact Information: Dr. Upal Ghosh, Department of Civil and Environmental Engineering, Stanford University, Stanford CA 94305. Email: ughosh@stanford.edu. Telephone: 650-723-5885. URL: http://www.stanford.edu/~ughosh

New IR microscope and bench installed at BL1.4

Michael C. Martin[a], Hoi-Ying N. Holman[b], and Wayne R. McKinney[a]
[a] Advanced Light Source Division, Lawrence Berkeley National Laboratory, Berkeley, CA 94720
[b] Center for Environmental Biotechnology, Lawrence Berkeley National Laboratory, Berkeley, CA 94720

1. INTRODUCTION

New infrared spectromicroscopy equipment was purchased for and installed on the ALS infrared beamlines on beam port 1.4. It includes the latest step-scan capable FTIR bench and an infinity corrected infrared microscope which will allow for a number of new sample visualization methods. This equipment was purchased with funding from the DOE Office of Biological and Environmental Research (OBER) with the express purpose to develop biomedical and biological applications of synchrotron-based infrared spectromicroscopy.

2. EQUIPMENT

The new spectromicroscopy equipment includes a Thermo Nicolet Nexus 870 step- and rapid-scan FTIR bench, and a Thermo Spectra-Tech Continuum IR microscope, photographed below. The IR microscope includes two IR detectors, a wide-band MCT and a fast (20 ns) TRS MCT for time-resolved experiments. A fast digitizer (up to 100MHz) compliments the TRS MCT detector. The synchrotron beam coupled into the IR microscope continues to have a diffraction-limited spot size, thereby attaining a 200-fold increase in signal from small (3 – 10 micron) sample spot compared to a conventional thermal IR source. The infinity-corrected microscope optics allow for a number of additional sample visualization accessories which can help the user identify the important location within their sample for micro-IR analysis:

- Visual and IR polarizers
- Dark-field illumination
- DIC (Differential Interference Contrast) optics
- UV Fluorescence

An example of DIC optics enhancing a micrograph of human cheek cells is shown in the photograph to the right. The DIC technique provides a psuedo-3D effect, enhancing the contrast between different thicknesses of an otherwise clear sample. In the image to the right, one can make out the nuclei of the cells (thicker bump near the middle of each cell), whereas this would be difficult using conventional illumination.

This new instrument will aide in user scientific research across many fields. For example, the study of individual living cells, toxic contaminants, bioremediation, protein microcrystals, rhizoids, and forensic evidence will all be enhanced by the additional capabilities of this new SR-FTIR spectromicroscopy system.

ACKNOWLEDGEMENTS

This research was supported by the Office of Science, Office of Biological and Environmental Research, Medical Science Division and the Office of Science, Office of Basic Energy Sciences, Materials Sciences Division, of the U.S. Department of Energy under Contract No. DE-AC03-76SF00098 at Lawrence Berkeley National Laboratory.

Principal investigator: Michael C. Martin, Advanced Light Source Division, LBNL, 510-495-2231, MCMartin@lbl.gov

Spatial Distribution of Bacteria on Basalt Using SR-FTIR

Mary E. Kauffman,[†,1,2] Hoi-Ying Holman,[3] R. Michael Lehman,[2] Michael C. Martin[4]

[1]Idaho State University, Depts. Of Biologiy and Geology, Pocatello, ID, 83209, [2]Idaho National Engineering and Environmental Laboratory (INEEL), Idaho Falls, ID, 83415, [3]Center for Environmental Biotechnology, Lawrence Berkeley National Laboratory, Berkeley, CA, 94720, [4]Advanced Light Source, Lawrence Berkeley National Laboratory, Berkeley, CA, 94720. [†]Address correspondence to Mary E. Kauffman, INEEL, Geomicrobiology Group, PO Box 1625, MS 2203, Idaho Falls, ID, 83415. Email:kaufme@inel.gov

INTRODUCTION

Understanding the role of microorganisms on the fate and transport of contaminants is essential in the determination of risk assessment and the development of effective remediation strategies for contaminated sites. The microscale distribution of microorganisms on the surface of complex geologic media will affect the types and rates of biotransformations in contaminated environmental systems. In this study, we used synchrotron radiation-based Fourier transform infrared spectromicroscopy (SR-FTIR) at the Advanced Light Source (ALS) Beamline 1.4.3, Lawrence Berkeley National Laboratory (LBNL), to investigate the preferential attachment of *Burkholderia cepacia* G4 to the various mineral phases within basalt. SR-FTIR is a non-destructive, in situ analytical tool, that when coupled to an automated X, Y positioning stage, can provide surface mapping of biochemical functional groups.

MINERAL AND BASALT SPECIMENS

Basalt specimens were prepared from core samples. The center of the core was cut into 1” square blocks and then sliced into specimens 1 mm thick using a diamond saw blade and water as the lubricant. Mineral standards for the four major mineral phases in basalt (plagioclase, augite, ilmenite and olivine) were prepared in the same fashion. The specimens were sonicated and autoclaved prior to use. Basalt and mineral specimens were spectrally characterized using SR-FTIR prior to, and after, exposure to a bacterial growth culture for several days. SR-FTIR spectra

of the distinct mineral phases in the basalt were compared to spectra obtained for individual mineral standards.

BACTERIAL CELLS, CULTURES AND CONDITIONS

Burkholderia cepacia G4 was selected as the model organism for this study due to the fact that it is a common soil microorganism, and therefore representative of bacteria found in environmental systems. Microcosms consisting of basalt or mineral specimens and bacterial culture solution were placed on a rotary shaker (55 rpm) at 23 ° C for five days. The culture solutions were changed daily and new inoculum was added. At the end of the five days, the specimens were removed from solution and rinsed with phosphate buffer to remove any loose cells.

SR-FTIR SPECTROMICROSCOPY

SR-FTIR spectra were collected at Beamline 1.4.3 at the ALS, LBNL, Berkeley, CA. All SR-FTIR spectra were recorded in the 4000-650 cm^{-1} infrared region. This region contains absorbance features correlative to characteristic IR-active vibrational modes for common biomolecules such as nucleic acids, proteins and lipids, as well as identifying absorbance features for the basalt and mineral specimens. Spectral maps of the basalt surfaces were obtained by programming the microscope X-Y positioning stage to collect spectra at specific step locations and then extracting spatial information of functional groups based upon absorbance peak wavenumbers. Data was collected in single-beam reflectance mode with a spectral resolution of 4 $cm^{-1}$and 64 scans were co-added for Fourier transform processing for each spectrum. Each resulting spectrum was then ratioed to the spectrum of a gold slide to produce absorbance values. By extracting each individual spectrum within the mapping grid and comparing it to spectra collected on each of the four individual minerals, identification of the underlying mineralogy can be determined. Figure 1 shows the spatial distribution of bacteria on a basalt surface, based upon the occurrence of the protein amide I peak at ~1650 cm^{-1}, and the preferential attachment by *B. cepacia* G4 to plagioclase. The total map area was 250 X 105 μm

with spectra collected every 25 µm along the X coordinate and every 15 µm along the Y coordinate. Correlative maps of the same surface area were constructed based upon the protein amide II peak at ~1550 cm^{-1} and at least one other absorbance feature related to the presence of biomolecules, to insure the resulting map was due to the spatial distribution of bacteria and not an artifact of the mineralogy (data not shown).

RESULTS

Multiple SR-FTIR maps of basalt surfaces colonized by bacterial cultures showed preferential attachment by *B. cepacia* G4 to plagioclase within the basalt matrix. The mineral apatite ($Ca_5(PO_4)_3(F, Cl, OH)$) is a common accessory mineral in igneous rocks and appears as inclusions in igneous plagioclase feldspars. Phosphorous is required by bacterial cells for the synthesis of nucleic acids and phospholipids. Scanning electron microprobe results indicate the presence of phosphorous in both the plagioclase within the basalt matrix and in the Ward's standard plagioclase specimen (data not shown). A recent study on feldspars as a source of nutrients determined that microorganisms extracted inorganic phosphorous from apatite inclusions in alkaline feldspars. It is highly likely that *B. cepacia* G4 preferentially attaches to the calcic plagioclase in order to access phosphorous from apatite inclusions.

This work was supported by the Idaho National Engineering and Environmental Laboratory.

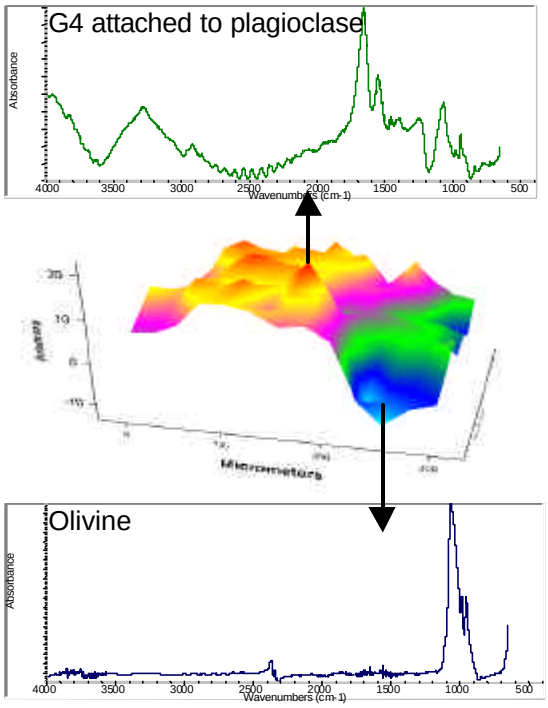

Figure 1.

Surface spectroscopy of nano-scale reactions in aqueous solution

K. H. Pecher[1,2] and B. Tonner[2]
[1]currently at: Advanced Light Source, Ernest Orlando Lawrence Berkeley National Laboratory, University of California, Berkeley, California 94720, USA
[2]Depaartment of Physics, University of Central Florida, Orlando, Florida 32816-2385, USA

INTRODUCTION

The rate of oxidation of dissolved Mn(II) by oxygen is enhanced in the presence of catalytic surfaces. Surfaces of iron oxides such as Goethite (α-FeOOH), Lepidocrocite (γ-FeOOH), and Hematite (α-Fe_2O_3) can increase the rate of Mn(II) oxidation over the initial homogeneous solution rate by orders of magnitude [1, 2]. These reactions are further complicated by the observation that initially formed reaction products are metastable and depend strongly on both the bulk reaction conditions such as temperature, concentration of Mn(II), pH-value, presence of dominant anions [3-5], and interfacial reaction conditions existing at the catalytic surfaces. The activities of reactants and products and especially the thermodynamic properties of Mn(III) species at such surfaces are not known and are not readily measurable [4]. In addition, initially formed Mn-oxides or hydroxides may autocatalytically enhance reaction rates [6]. A contribution from autocatalytic oxidation of Mn(II) has been hypothesized for the formation of Mn-micronodules in lake sediments [7] and the occurrence of Mn-biominerals formed by spores of a marine bacillus *SG-1* [e.g. 8, 9]. It is therefore quite natural that details on the identity of reaction products vary a lot in the literature.

Traditionally, two different approaches have been utilized to study Mn(II) oxidation at mineral surfaces: a macroscopic approach using wet chemistry data and surface complexation models [10], and a microscopic approach using Scanning Force Microscopy and surface spectroscopic techniques [11]. Junta-Rosso et al. [12] have also tried to link both microscopic and macroscopic data to develop rate expressions that are consistent with both approaches. The microscopic as well as surface spectroscopic techniques applied in those studies suffer from transfer of wet samples into high vacuum, the effect of which has not yet been studied systematically. We have used Scanning Transmission X-ray Spectromicroscopy (STXM) to characterize products formed during the heterogeneous oxidation of Mn(II) by dissolved oxygen on fully hydrated single nano-sized particles of catalytically active iron oxides.

MATERIALS AND METHODS

Aliquots of powdered iron oxides (Goethite, Lepidocrocite, and Hematite) equivalent to 25 m^2L^{-1} were each suspended in 10 mM HEPES solution (pH 7.8, 50 mM NaCl) and equilibrated for 24 h. Characteristics of the used iron oxides are given elsewhere [13]. These suspensions were kept open to atmosphere on a multi stirring plate and were repeatedly spiked with aliquots from a 55 mM $MnCl_2$ stock solution. Time intervals between sequential addition of Mn(II) were chosen long enough to keep the concentration of dissolved Mn(II) below 0.3 mM.
Two sets of samples were withdrawn for STXM measurements: (a) after 96 d of reaction time and a total Mn(II)-dosage of 244 μM, and (b) after 129 d of reaction time and a total Mn(II)-dosage of 1.26 mM. All X-ray absorption measurements were done at the Advanced Light Source (Lawrence Berkeley National Laboratory) on beam line 7.0.1. Sample preparation and

technical specifications of an upgrade version of STXM are given elsewhere [14, 15]. Data analysis and spectral interpretation using XANES of reference compounds are detailed in [16].

RESULTS AND DISCUSSION

STXM of the first set of samples withdrawn after 96 days and a total Mn(II) dose of 244 μM, did not result in detectable amounts of Mn on the iron oxide particles. Obviously, the mass of adsorbed Mn(II) and/or oxidation products present on the particles were below the detection limit of the instrument. Figure 1 shows single needles of Goethite after 129 d of incubation imaged at the Fe absorption maximum and the corresponding XANES of the Mn-edge. The spectrum could be fitted by a linear combination of spectra of single valent Mn(II) and Mn(III)-reference models. Fits did not improve by including any Mn(IV)-component.

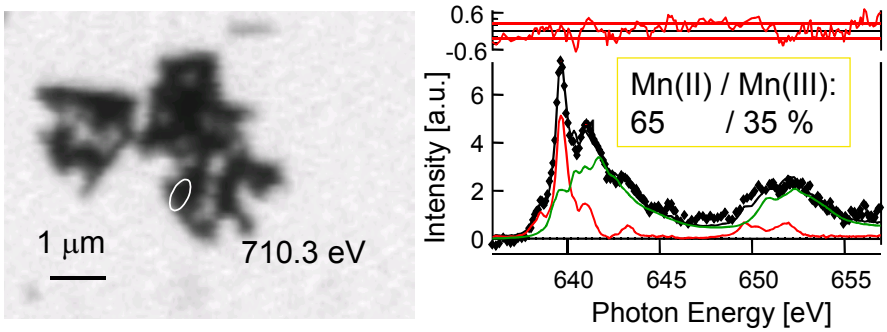

Figure 1. Image of single needles of Goethite (left) and XANES (◆) at the Mn-edge extracted from the area labeled on the image. The XANES is fitted to a linear combination of spectra of single valent reference compounds (red: $MnSO_4$, green: γ-MnOOH). Quantitative results are given in mass % of each charge component and residuals are plotted with the horizontal lines indicating ± one standard deviation.

Under the experimental conditions used, the iron oxide catalyzed oxidation of Mn(II) led to a mixed valent Mn(II)/Mn(III)-species (most likely Hausmannite [4,5]), the stoichiometric ratio of which might be superimposed by specific adsorption of Mn^{2+} from solution. Control experiments under anoxic conditions are necessary to decide whether the high Mn(II)-content is due to adsorption of Mn^{2+} onto iron oxide surfaces or incorporation into oxidation products. Within the time frame of our experiment, we can rule out disproportionation of initial Mn(III)-species, although this reaction is thermodynamically favorable under our bulk reaction conditions. We hypothesize that reaction conditions at the iron oxide interfaces can stabilize Mn(III). Comparing the mass fraction of Mn(III) on all three iron oxides, the order is α-FeOOH»α-Fe_2O_3>γ-FeOOH, which does not correlate with the amount of specific sites for cation sorption on those oxides. The observed order, however, does correlate with the order of catalytic activities observed during reductive dehalogenation of polyhalogenated methanes by Fe(II) sorbed to exactly the same iron oxides [13]. We conclude that unknown steric/electronic properties of the iron oxide substrates might be involved as controlling factors in lowering the redox potential of transition metal cations sorbed to such surfaces.

ACKNOWLEDGMENTS

Thanks to Sirine Fakra, Rick Steele and Tony Warwick for providing such a wonderful instrument. Adam Hitchcock and Eli Rotenberg provided software for data analysis.

REFERENCES

[1] Diem, D.; Stumm, W. Geoch. et Cosmoch. Acta 1984, 48,1571-1573.
[2] Sung, W.; Morgan, J.J. Geoch. et Cosmoch. Acta 1981, 45,2377-2383.
[3] Hem, J.D. Geoch. et Cosmoch. Acta 1981, 45,1369-1374.
[4] Hem, J.D.; Lind, C.J. Geoch. et Cosmoch. Acta 1983, 47, 2037-2046.
[5] Murray, J.W.; Dillard, J.G.; Giovanoli, R.; Moers, H.; Stumm, W. Geoch. et Cosmoch. Acta 1985, 49,463-470.
[6] Murray, J.W. Geoch. et Cosmoch. Acta 1975, 39,505-519.
[7] Murray, L.W.; Balistrieri, L.S.; Paul, B. Geoch. et Cosmoch. Acta 1984, 48,1237-1247.
[8] Nealson, K.H.; Tebo, B.M. Adv. Appl. Microbiol. 1988, 33,279-318.
[9] Mandernack, K.W.; Post, J.; Tebo, B.M. Geoch. et Cosmoch. Acta 1995, 59,4393-4408.
[10] Davies, S.H.R.; Morgan, J.J. J. Colloid Interface Sci. 1989, 129,63-77.
[11] Junta, J.L.; Hochella Jr., M.F. Geochim. Cosmochim. Acta 1994, 58,4985-4999.
[12] Junta-Rosso, J.L.; Hochella Jr., M.F.; Rimstidt, J.D. Geoch. et Cosmoch. Acta 1997, 61,149-159.
[13] Pecher, K.; Haderlein, S. B.; Schwarzenbach, R. P. Environ. Sci. Technol. 2001 accepted.
[14] http://www-esg.lbl.gov/Stxm/
[15] Pecher, K.; Kneedler, E.; Rothe, J.; Meigs, G.; Warwick, T.; Nealson, K.; Tonner, B. In: X-ray Microscopy (XRM´99); AIP Conference Proceedings 507, W. Meyer-Ilse, T. Warwick, D. Attwood (Eds.); Berkeley, 2000; p 291-300.
[16] Pecher, K.; McCubbery, D., Kneedler, E.; Rothe, J.; Bargar, J.; Meigs, G.; Cox, L., Nealson, K.; Tonner, B. submitted to Geoch. et Cosmoch. Acta 2001.

This work was supported by the Director, Office of Energy Research, Office of Basic Energy Sciences, Materials Science Division, of the U.S. Department of Energy under Contract No. DE-AC03-76SF00098. This work was supported by grants from DOE Division of Materials Sciences FG02-98ER45688 and DOE NABIR FG02-97ER62474.

Principal investigator: Klaus Pecher, Advanced Light Source, Ernest Orlando Lawrence Berkeley National Laboratory. Email: khpecher@lbl.gov. Telephone: 510-495-2232.